

Selective oxidation of sulfides with oxygen over a pyrene covalent organic framework photocatalyst with TEMPO

Xiaoyun Dong, Fulin Zhang, Yuexin Wang, Fengwei Huang, Xianjun Lang*

Hubei Key Lab on Organic and Polymeric Optoelectronic Materials, College of Chemistry and Molecular Sciences, Wuhan University, Wuhan 430072, China



ARTICLE INFO

Keywords:
Photocatalysis
Azine
Semiconductor
Blue light
Hole mediator

ABSTRACT

Covalent organic frameworks (COFs) can be precisely modulated through the covalent linkage of organic building blocks. Therefore, developing COFs to high-performance photocatalysts is highly applicable. Herein, with trifluoroacetic acid as the catalyst, Py-Azine-COF is constructed by aldimine condensation between 1,3,6,8-tetrakis(4-formylphenyl)pyrene and hydrazine hydrate. The highly crystalline Py-Azine-COF possesses a remarkable specific surface area of $1428 \text{ m}^2 \text{ g}^{-1}$. Intriguingly, selective aerobic conversion is achieved over Py-Azine-COF photocatalyst with (2,2,6,6-tetramethylpiperidin-1-yl)oxyl (TEMPO). Significantly, TEMPO accelerates the hole transfer and cooperates with superoxide formed from oxygen for selective oxidation of organic sulfides. With the assistance of 2 mol% TEMPO, the performance of Py-Azine-COF photocatalyst is increased markedly. Gratifyingly, TEMPO, a hole mediator, enables expeditious conversions of various sulfides into sulf-oxides over Py-Azine-COF photocatalyst in methanol. Generally, COFs can be customized by modulating the covalent connection of organic building blocks to meet the requirements of selective aerobic oxidations.

1. Introduction

Covalent organic frameworks (COFs), a class of crystalline and porous materials with extended π -conjugated structures, were successfully established and first reported in 2005 [1]. This work provides impetus for the ongoing exploration of COFs [2–5]. So far, substantial advancements have been made in aspects of reticular topologies and covalent linkages [6–10]. Moreover, the precise modulation of organic building blocks at the molecular level allows for tailor-made COFs to acquire desired optoelectronic properties, further enriching the diversity of COFs [11,12]. Besides, the well-ordered arrangements of organic building blocks and covalent linkages endow COFs with permanent and periodic porosity, large specific surface area, and good stability [13–16]. Till now, these merits enable COFs to be widely exploited for various fields, including biomedicine [17], catalysis [18,19], environmental remediation [20], gas adsorption [21,22], and energy storage [23–25]. Particularly, COFs present tremendous potential in visible light photocatalysis, such as H_2O_2 production [26,27], CO_2 reduction [28,29], H_2O splitting [30], H_2 evolution [31], and organic transformation [32–37], emerging as an up-and-coming candidate to tackle issues in environment and energy.

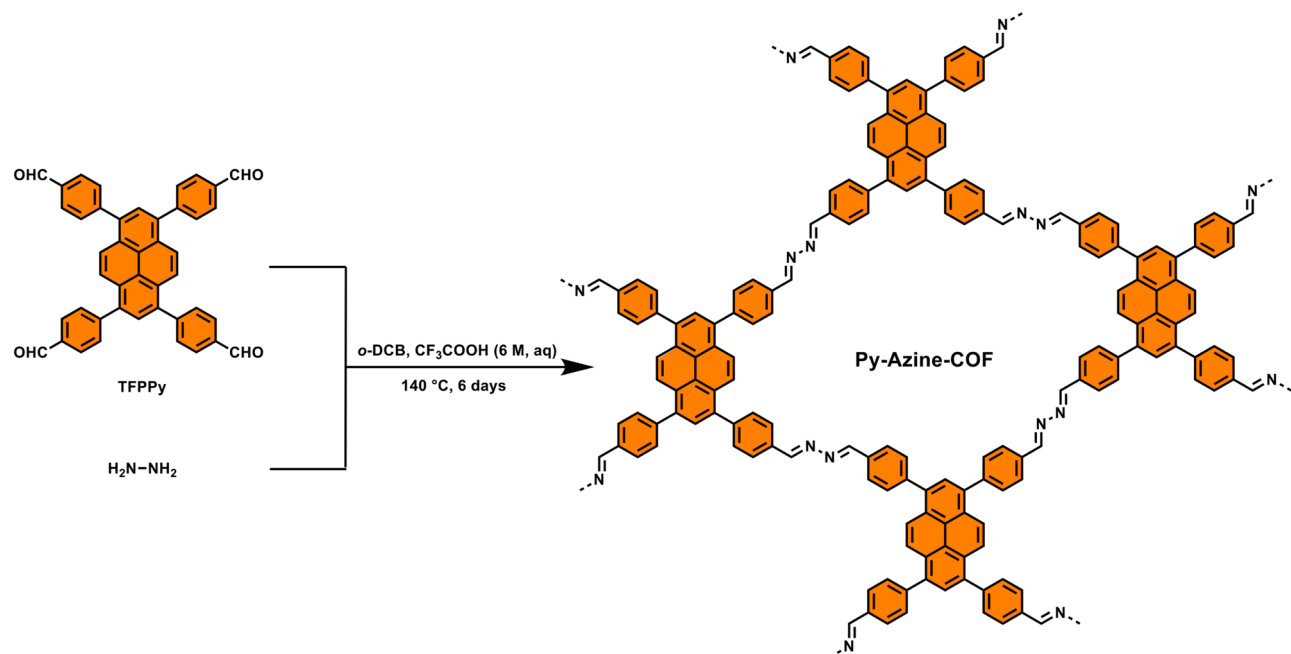
Pyrene, a polycyclic aromatic hydrocarbon, has shown bright

prospects as a chromophore for regulating light absorption of its afforded porous materials [38–43]. Incorporating the bulky π -conjugated system of pyrene skeleton allows the facile separation and migration of charge carriers, thus enhancing their optoelectronic property significantly [44–46]. In parallel, the planar structure of pyrene skeleton is able to strengthen interlayer π – π interaction effectively and ameliorate the crystallinity and stability of COFs [47–49]. As yet, multitudinous pyrene-based conjugated microporous polymers and metal–organic frameworks have been explored for photocatalysis, exhibiting remarkable performance in many cases [50–52]. These facts fully underpin that pyrene is an outstanding photoactive building block for COFs. As such, the exploration of a suitable covalent linkage for pyrene is paramount for customizing high-performance COF photocatalysts. Among the numerous covalent linkages, the azine bond ($-\text{C}=\text{N}-\text{N}=\text{C}-$) derived from the dynamic imine bond not only retains its original function of “error correction”, but also expands its π -conjugated structure, enhancing chemical stability effectually [53,54]. Importantly, azine linkage can be easily accessible by the prevalent aldimine condensation [55]. Thus, it is expected to construct a pyrene COF photocatalyst using azine as the linkage.

In this vein, pyrene building block and azine linkage are selected to construct a pyrene COF. Using trifluoroacetic acid (CF_3COOH) as the

* Corresponding author.

E-mail address: xianjunlang@whu.edu.cn (X. Lang).



Scheme 1. Schematic for the construction of Py-Azine-COF.

catalyst, the aldimine condensation between 1,3,6,8-tetrakis(4-formylphenyl)pyrene (TFPPy) and hydrazine hydrate furnishes Py-Azine-COF with the pyrene skeleton and azine linkage (Scheme 1). The characterization results show that the highly crystalline Py-Azine-COF is an n-type semiconductor, exhibiting a remarkable specific surface area of $1428 \text{ m}^2 \text{ g}^{-1}$. Intriguingly, the performance is improved over Py-Azine-COF photocatalyst with (2,2,6,6-tetramethylpiperidin-1-yl)oxyl (TEMPO). In essence, as a hole mediator, TEMPO accelerates the charge transfer generated by photoexcited Py-Azine-COF photocatalyst and cooperates with superoxide (O_2^-), formed by electron transfer from oxygen (O_2), to accomplish selective oxidation of organic sulfides. With the assistance of 2 mol% TEMPO, the performance of Py-Azine-COF photocatalyst is increased markedly during selective oxidation of organic sulfides under blue light irradiation. Gratifyingly, TEMPO, a hole mediator, enables expeditious conversions of various sulfides into sulfoxides over Py-Azine-COF photocatalyst in methanol (CH_3OH). In general, COFs can be customized by modulating the covalent connection of organic building blocks to meet the requirements for selective aerobic oxidations.

2. Experimental section

2.1. The construction of Py-Azine-COF

According to a previous report [54], Py-Azine-COF was constructed via aldimine condensation with slight modification. Importantly, using CF_3COOH , instead of acetic acid (CH_3COOH), as the catalyst ameliorated the crystallinity of Py-Azine-COF effectively. At first, TFPPy (0.045 mmol, 28.7 mg) and 85% aqueous solution of hydrazine hydrate (0.099 mmol, 5.7 μL) were uniformly dispersed in *o*-dichlorobenzene (*o*-DCB, 3 mL) in a Pyrex tube via ultrasonication. Then, an aqueous solution of 6 M CF_3COOH (0.1 mL) was rapidly added to the mixture. Subsequently, the Pyrex tube was sealed by flame under vacuum after the freeze–pump–thaw degassing cycles, followed by heating in an oven at 140°C for 6 days. Cooling the Pyrex tube to room temperature, the mixture in the tube was filtered. Then, the brown precipitate was gathered and rinsed with tetrahydrofuran and trichloromethane. Finally, Py-Azine-COF was collected as an orange and fluffy powder after drying in a vacuum oven at 100°C overnight. Elemental analysis

(%) for $(\text{C}_{44}\text{H}_{26}\text{N}_4)_n$, calculated: C 86.53, H 4.29, N 9.17; found: C 81.88, H 4.27, N 7.25.

2.2. The general procedure of photocatalysis

Under blue light irradiation, selective conversions of organic sulfides were implemented over Py-Azine-COF photocatalyst with TEMPO. Generally, the reaction system composed of CH_3OH (1 mL), TEMPO (6 μmol), methyl phenyl sulfide (0.3 mmol), and Py-Azine-COF (5 mg) was thoroughly stirred for 15 min under dark conditions. Then, irradiated by 460 nm blue LEDs (light-emitting diodes, 3 W \times 4), the system was filled with O_2 (0.1 MPa) to undergo conversion under continuous stirring. Next, with bromobenzene as an internal standard, the supernatant gathered by centrifugation was analyzed with a gas chromatograph collocated with a flame ionization detector (GC-FID) for qualitative and quantitative analyses. Further identification of the products was completed using gas chromatography–mass spectrometry (GC-MS).

3. Results and discussion

3.1. Characterizations for Py-Azine-COF

Aldimine condensation between TFPPy and hydrazine hydrate integrated the pyrene skeleton and azine linkage into a π -conjugated structure, giving rise to the construction of Py-Azine-COF (Scheme 1). Herein, the reaction parameters, such as temperature, solvent, and catalyst, were optimized to develop a pyrene COF with high crystallinity under the solvothermal conditions (Supplementary Table S1). It was found that the acid catalyst plays a decisive role in ameliorating the crystallinity of Py-Azine-COF (Supplementary Fig. S1). In detail, using CF_3COOH , instead of CH_3COOH , as the catalyst ameliorated the crystallinity of Py-Azine-COF effectively. Finally, with 6 M CF_3COOH as the catalyst, highly crystalline Py-Azine-COF was afforded in *o*-DCB at 140°C for 6 days, confirmed by powder X-ray diffraction (PXRD) analysis (Fig. 1a). The PXRD pattern showed that the afforded Py-Azine-COF under the optimized conditions possesses a long-range periodic structure. The diffraction peaks at 4.64° , 6.12° , 9.24° , 13.82° , and 23.38° were observed, ascribing to (110), (200), (220), (330), and (001) facets, respectively. According to the simulations of the lattice modeling of Py-

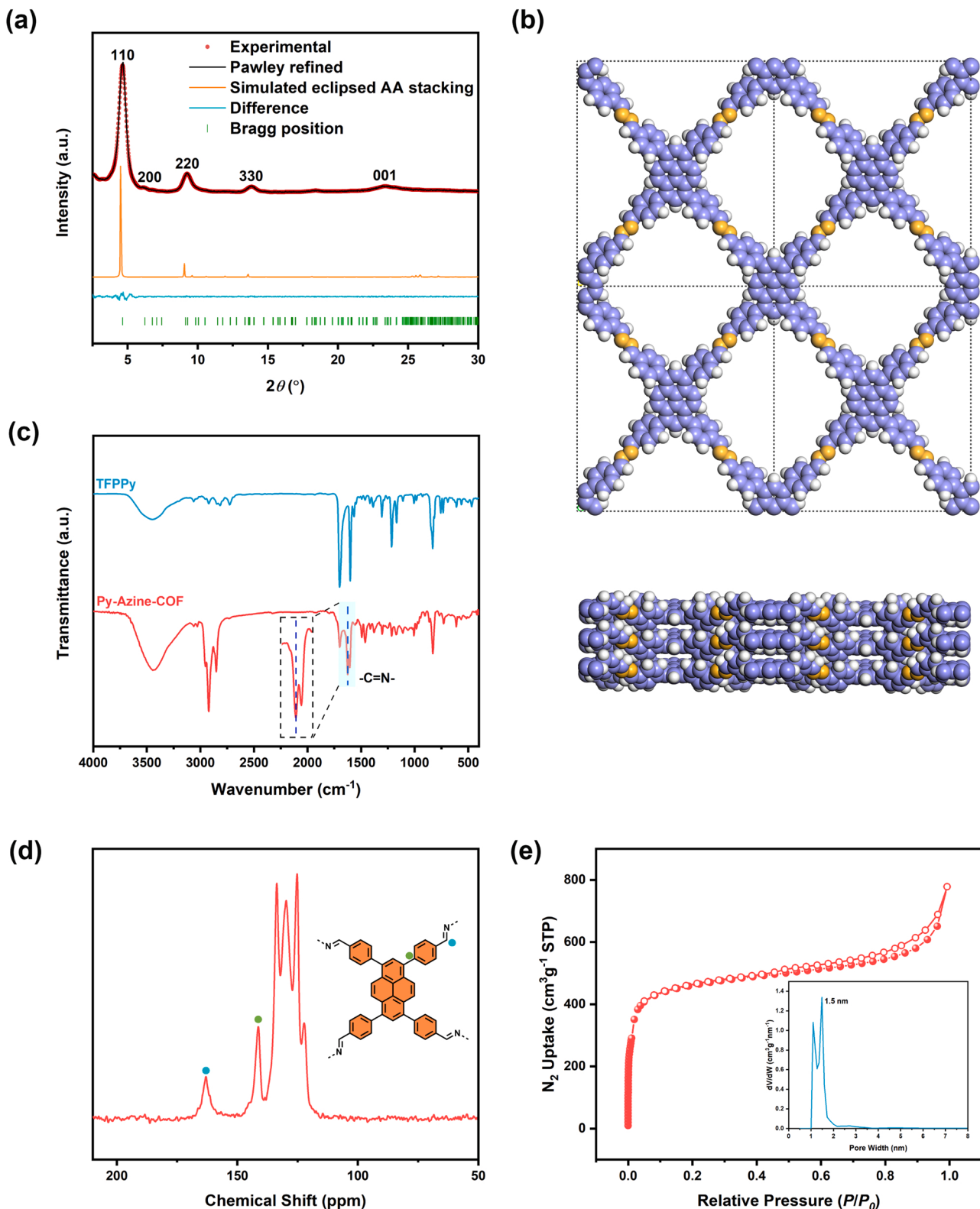


Fig. 1. (a) PXRD patterns of Py-Azine-COF: experimental profile in red, Pawley refined result in black, simulated eclipsed AA stacking mode in orange, the difference in blue, and Bragg positions in green. (b) The eclipsed lattice structure of Py-Azine-COF at top view (above) and side view (below). (c) FTIR spectra of Py-Azine-COF and TFPPy. (d) The solid-state ^{13}C NMR spectrum of Py-Azine-COF. (e) The N_2 sorption isotherms and corresponding pore size distribution curve of Py-Azine-COF.

Azine-COF, the experimental PXRD profile is in line with the PXRD pattern deduced from the eclipsed AA stacking mode (Fig. 1b). Besides, the observed experimentally PXRD pattern was reproduced via the Pawley refinement and their negligible difference was also presented

($R_{wp} = 3.99\%$ and $R_p = 3.07\%$). Also, Py-Azine-COF possessed a C_2/m space group with the cell unit parameters of $a = 26.0552 \text{ \AA}$, $b = 31.1636 \text{ \AA}$, $c = 3.6281 \text{ \AA}$, $\alpha = 71.78^\circ$, $\beta = \gamma = 90^\circ$. Importantly, five separate batches of Py-Azine-COF all displayed high crystallinity,

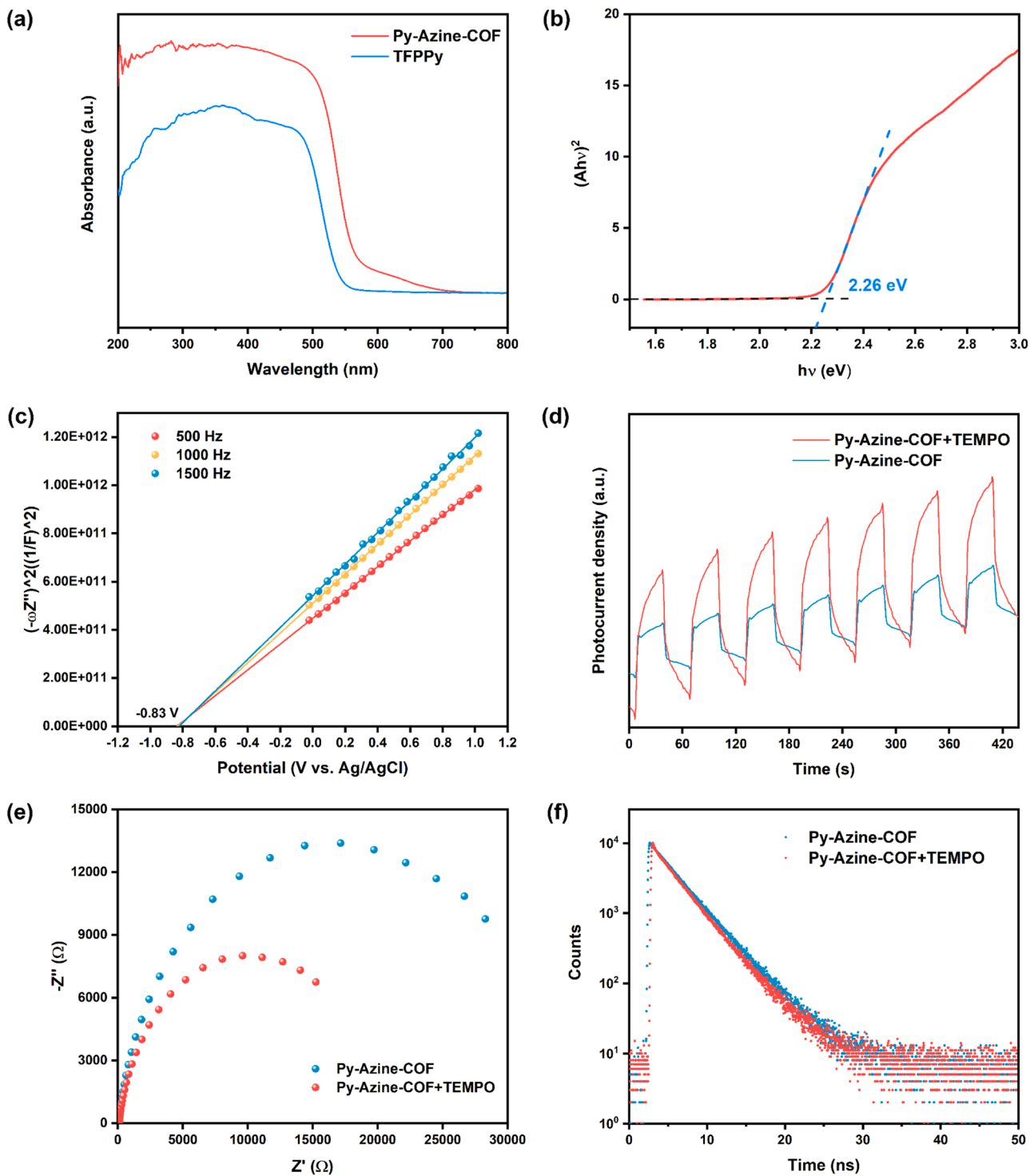


Fig. 2. (a) UV-visible DRS of Py-Azine-COF and TFPy. The corresponding Tauc plot (b) and the Mott-Schottky plots (c) of Py-Azine-COF. The transient photocurrent densities (d), the Nyquist plots of EIS (e), and time-resolved fluorescence decay (f) of Py-Azine-COF with or without TEMPO.

indicating the good reproducibility in constructing the COF under the typical conditions ([Supplementary Fig. S2](#)).

Further, Fourier transform infrared spectroscopy (FTIR) spectra disclosed the successful construction of highly crystalline Py-Azine-COF with the newly appeared absorption band of C=N bond at ca. 1622 cm^{-1} ([Fig. 1c](#)). Besides, the carbon signal of the formed C=N bond appeared at ca. 163.0 ppm in the solid-state ^{13}C nuclear magnetic resonance (NMR) spectrum of Py-Azine-COF ([Fig. 1d](#)). Also, the signal peak of the carbon on the benzene ring connected to pyrene in Py-Azine-

COF appeared at ca. 141.3 ppm . Next, field emission-scanning electron microscopy (FE-SEM) image displays a morphology of clear nanorods of micron lengths for Py-Azine-COF, which was also proved by the high-resolution transmission electron microscopy (HR-TEM) image ([Supplementary Figs. S3 and 4](#)). More importantly, a regular arrangement was observed and the corresponding line intensity profile revealed the pore size of about 1.59 nm for Py-Azine-COF. By the nitrogen (N_2) sorption isotherms, the porosity of Py-Azine-COF was evaluated ([Fig. 1d](#)). Py-Azine-COF preserved a characteristic type IV isotherm, which is

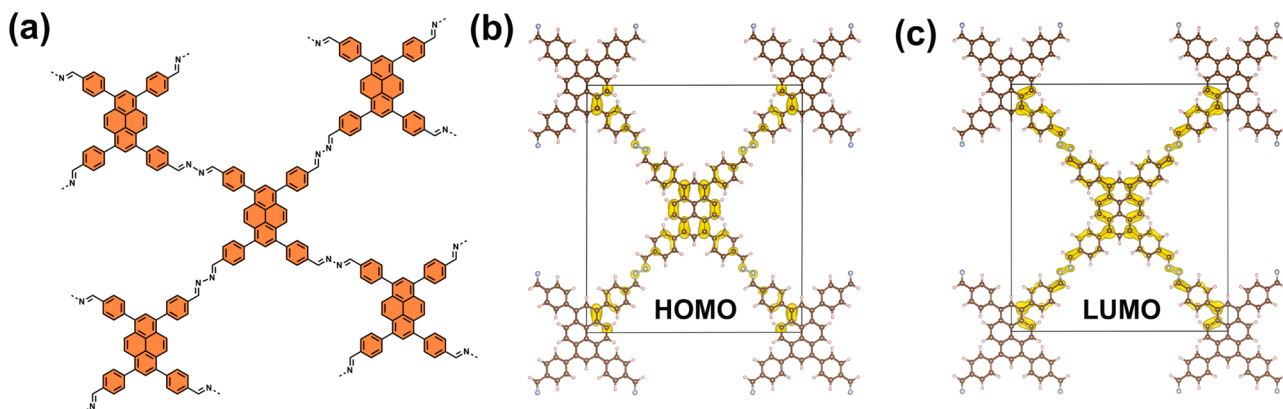


Fig. 3. (a) The simplified molecular structure of Py-Azine-COF. The calculated charge density distributions of HOMO (b) and LUMO (c) of Py-Azine-COF.

consistent with microporosity. By fitting nonlocal density functional theory (DFT) models to the above type IV isotherm, the pore size derived for Py-Azine-COF mainly distributed around 1.5 nm, which is very close to the pore size determined by the line intensity profile of the HR-TEM

image (Supplementary Fig. S4). Moreover, the Brunauer–Emmett–Teller specific surface area of Py-Azine-COF was determined as $1428 \text{ m}^2 \text{ g}^{-1}$ and the pore volume was assessed as $0.96 \text{ cm}^3 \text{ g}^{-1}$. Also, when the temperature rose to 600°C in the thermogravimetric analysis test, 85%

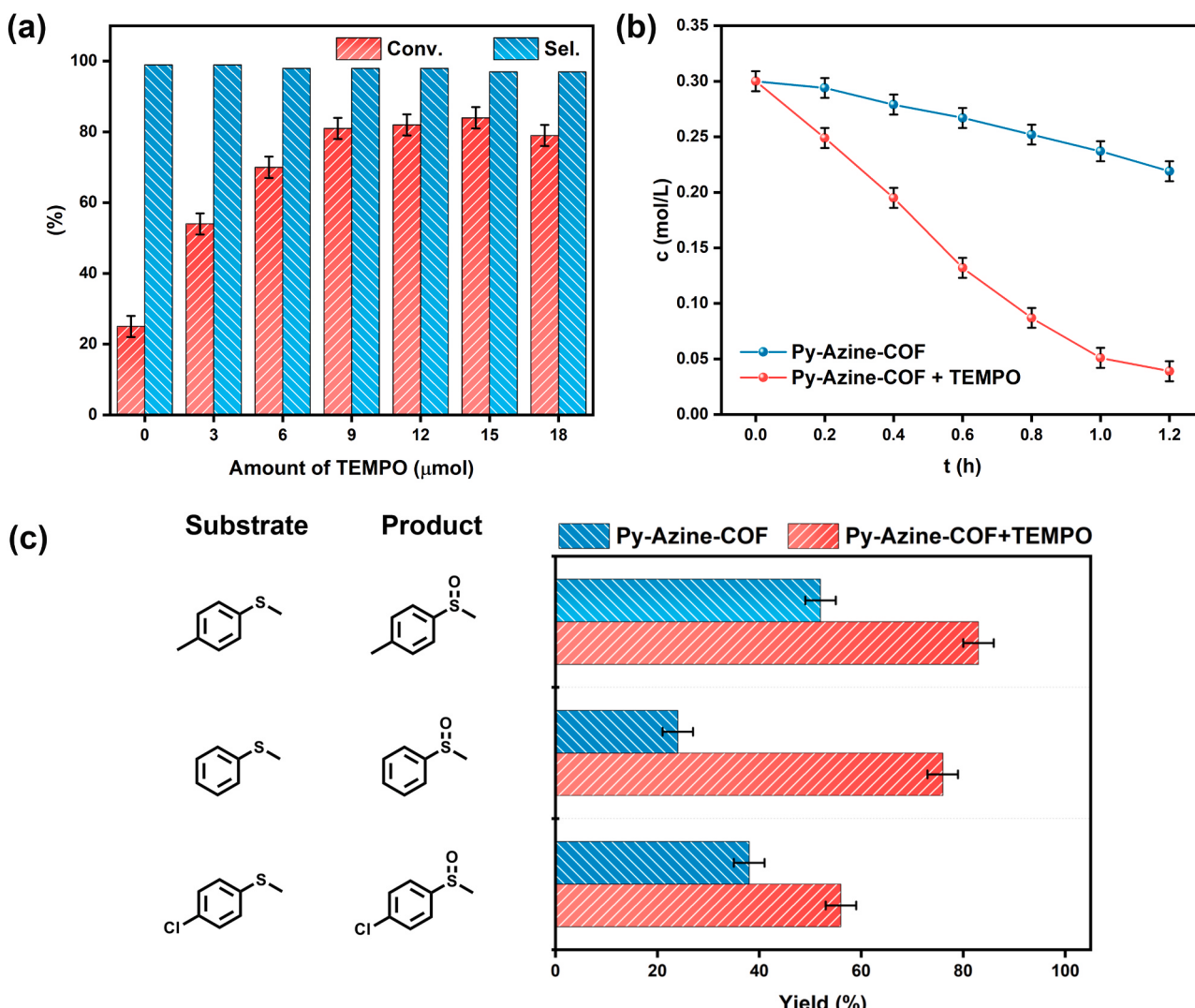


Fig. 4. (a) The effect of TEMPO amount on the selective oxidation of methyl phenyl sulfide over Py-Azine-COF photocatalyst. (b) Kinetic curves for the selective oxidation of methyl phenyl sulfide over Py-Azine-COF photocatalyst with or without TEMPO, respectively. (c) The effect of 2 mol% TEMPO on the selective oxidation of three methyl phenyl sulfides over Py-Azine-COF photocatalyst. Standard conditions: Py-Azine-COF (5 mg), CH_3OH (1 mL), TEMPO (6 μmol), methyl phenyl sulfide (0.3 mmol), blue LEDs ($\lambda_p = 460 \text{ nm}$), O_2 (0.1 MPa). Reaction time: (a) 0.8 h; (c) 1.1 h.

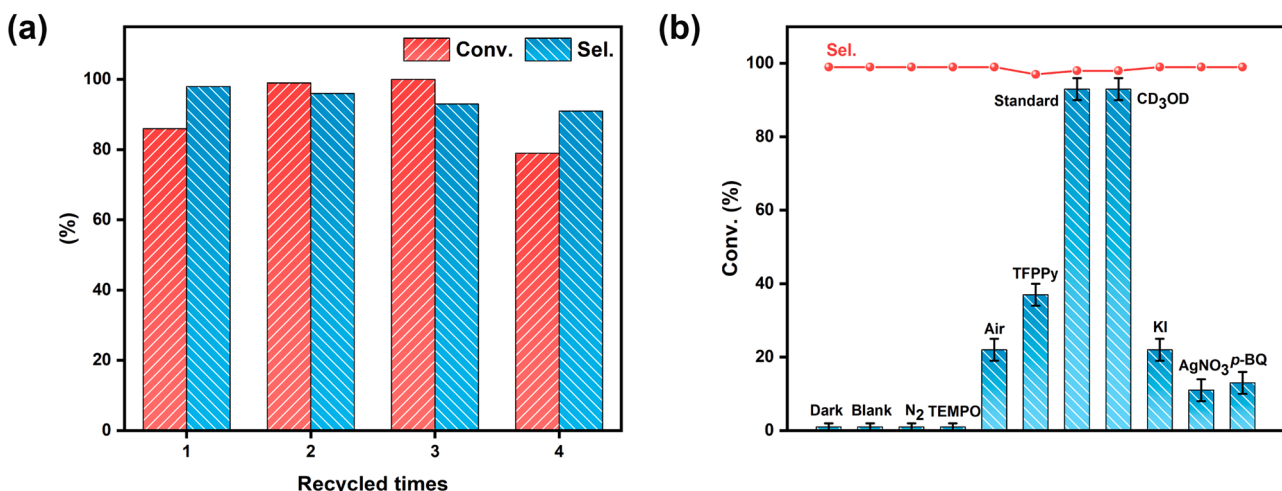


Fig. 5. (a) Recycling of Py-Azine-COF photocatalyst for the selective oxidation of methyl phenyl sulfide. (b) Control and quenching tests for selective oxidation of methyl phenyl sulfide over Py-Azine-COF photocatalyst. Standard conditions: Py-Azine-COF (5 mg), CH_3OH (1 mL), TEMPO (6 μ mol), methyl phenyl sulfide (0.3 mmol), blue LEDs ($\lambda_p = 460$ nm), O_2 (0.1 MPa). Reaction time: (a) 1.2 h; (b) 1.5 h.

of the weight was still retained, indicating the established good stability of Py-Azine-COF (Supplementary Fig. S5).

The UV-visible diffuse reflectance spectrum (DRS) of Py-Azine-COF exhibited a broader visible light absorption range from 200 to 700 nm compared with that of TFPPy (Fig. 2a). Also, the property of direct semiconductor for Py-Azine-COF was further revealed because the value of n was determined to be 1/2, and the optical band gap was calculated as 2.26 eV in accord with the corresponding Tauc plot (Fig. 2b). The positive slope of Mott-Schottky plots obtained under different frequencies of 500, 1000, and 1500 Hz revealed that Py-Azine-COF is an n-type semiconductor, and its flat-band potential was decided as -0.83 V (Fig. 2c). The onset reduction potential of Py-Azine-COF was calibrated and further determined as -0.53 V versus $Ag/AgCl$ in the light of the cyclic voltammetry (CV) curve (Supplementary Figs. S6 and 7). In contrast to the potential of -0.48 V versus $Ag/AgCl$ for O_2/O_2^- couple, the more negative reduction potential enables the activation of ground state O_2 over Py-Azine-COF photocatalyst, further affording $O_2^\bullet-$. As such, the lowest unoccupied molecular orbital (LUMO) level of Py-Azine-COF was figured out to be -3.89 eV versus the vacuum (Supplementary Fig. S8). Further, the highest occupied molecular orbital (HOMO) level was calculated as -6.15 eV versus the vacuum. Meanwhile, the HOMO potential of Py-Azine-COF was calculated as $+1.65$ V versus normal hydrogen electrode (NHE). Compared to the oxidation potential of TEMPO/TEMPO $^+$ (0.75 V versus NHE) [56], the more positive HOMO potential indicates that Py-Azine-COF drives the transformation from TEMPO to TEMPO $^+$ (2,2,6,6-tetramethylpiperidine-1-oxoammonium). Besides, the effect of TEMPO on the redox potential of Py-Azine-COF was explored through CV curves (Supplementary Fig. S6). The results showed that the introduction of TEMPO indeed mediates charge transfer. Explicitly, because of the matched band positions, the generation of $O_2^\bullet-$ occurs over Py-Azine-COF via the activation of O_2 in the ground state, and TEMPO mediates the hole transfer generated by photoexcited Py-Azine-COF.

Subsequently, the charge separation and migration properties of Py-Azine-COF were explored through a series of photoelectrochemical tests. Gratifyingly, when a small amount of TEMPO was added to the organic electrolyte, the cathodic photocurrent density for Py-Azine-COF under blue light irradiation almost doubled compared to that without TEMPO (Fig. 2d). Moreover, using electrochemical impedance spectroscopy (EIS), a smaller arc radius was obtained in the Nyquist plot in the presence of TEMPO (Fig. 2e). The results indicated that TEMPO reduces the interfacial transfer resistance for charge carriers, giving rise to more efficient charge separation and migration over Py-Azine-COF. Further,

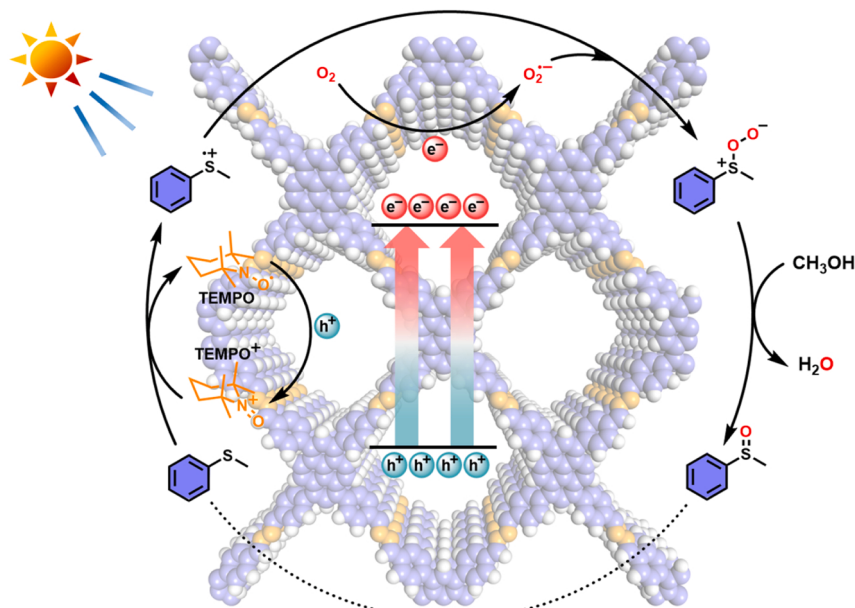
the introduction of TEMPO resulted in a reduction in average lifetime of Py-Azine-COF from the original 3.39 ns to 3.18 ns (Fig. 2f), indicating that TEMPO quenches the photoexcited Py-Azine-COF for charge transfer.

The charge distribution behavior of Py-Azine-COF was explored theoretically by DFT calculations based on a simplified model structure (Fig. 3a and Supplementary Fig. S9). The charge density distribution showed that the HOMO is confined to the pyrene skeleton, and the LUMO is relatively distributed on the pyrene skeleton and the azine linkage (Fig. 3b and c). On closer inspection, partial charge density on pyrene gradually shifted toward the azine linkage. The tendency indicates the attendance of a photoexcited state of charge transfer over Py-Azine-COF [57,58]. Besides, a possible locally excited state is manifested by virtue of the most overlap of charge density distribution between the HOMO and LUMO.

3.2. Selective oxidation of sulfides over Py-Azine-COF photocatalyst

Organic sulfoxides are valuable intermediates that are widely used in the synthesis of active pharmaceutical ingredients and reaction auxiliaries [59–64]. Selective photocatalytic oxidation of sulfides is an attractive avenue to obtain the highly valuable sulfoxides by controlling the generation of reactive oxygen species (ROS). Specifically, the nucleophilic attack of organic sulfide radical cation by $O_2^\bullet-$ can ensure the high selectivity of sulfoxides [65,66]. To date, Py-Azine-COF has never been applied in photocatalysis. Coincidentally, the LUMO potential of Py-Azine-COF can enable the generation of $O_2^\bullet-$. Thus, Py-Azine-COF was adopted as a photocatalyst for the activation of O_2 and subsequent oxidation reactions. Therefore, the performance of Py-Azine-COF photocatalyst was assessed through the selective oxidation of sulfides into sulfoxides. The transformation of methyl phenyl sulfide was chosen as the probe reaction.

Under blue light irradiation, Py-Azine-COF photocatalyst alone exhibited comparatively low performance. A conversion of 25% and an excellent selectivity were given (Fig. 4a). Delightedly, TEMPO, a hole mediator, established an obvious cooperative effect with Py-Azine-COF photocatalyst, boosting its performance dramatically. Moreover, the rise of TEMPO amount in the photocatalytic system led to a gradual increase in the conversion of methyl phenyl sulfide until the conversions entered a plateau and even rebounded slightly with further increase of TEMPO. Based on comprehensive consideration, 2 mol% TEMPO was deemed suitable for subsequent investigations. Then, the effect of 2 mol% TEMPO on the selective oxidation of methyl phenyl sulfide over Py-



Scheme 2. A proposed mechanism for selective oxidation of methyl phenyl sulfide with O_2 over Py-Azine-COF photocatalyst with TEMPO.

Azine-COF photocatalyst was further studied by the kinetic curves (Fig. 4b). The results showed that the selective oxidation of methyl phenyl sulfide over Py-Azine-COF photocatalyst almost obeys zero-order kinetics in the initial stage of conversion before 1.0 h with or without adding 2 mol% TEMPO. Importantly, selective oxidation of methyl phenyl sulfide was boosted with TEMPO over Py-Azine-COF photocatalyst, resulting in a three-fold conversions within 1.0 h. Besides, the effect of 2 mol% TEMPO on the selective oxidation of three methyl phenyl sulfides was explored over Py-Azine-COF photocatalyst (Fig. 4c). The boosting effect of the 2 mol% TEMPO on the selective oxidation of three sulfides was shown over Py-Azine-COF photocatalyst. The results all suggested that Py-Azine-COF photocatalysis cooperates with TEMPO to obtain higher conversions.

Additionally, the recyclability of Py-Azine-COF photocatalyst was further explored (Fig. 5a). It was found that Py-Azine-COF could be recycled at least four times with only a slight decline in performance. It is worth noting that the conversions of methyl phenyl sulfide in the second and third cycles were slightly higher than that in the first cycle. Likely, the agitation in the first cycle caused the slight exfoliation of $\pi-\pi$ stacking layers of Py-Azine-COF, which resulted in more exposed active sites. The PXRD pattern of the collected Py-Azine-COF after one cycle revealed its high crystallinity was fully preserved, and no obvious change in morphology was observed (Supplementary Figs. S10–S12). More importantly, the crystal structure of Py-Azine-COF was preserved after four cycles. Likewise, the characteristic absorption bands were completely kept as indicated by the FTIR spectrum of the collected Py-Azine-COF after one cycle (Supplementary Fig. S13). Nevertheless, for collected Py-Azine-COF after four cycles, the peak intensity of $-C=N-$ bond attenuated, which might be ascribed to the collapse of some local structures of Py-Azine-COF.

Moreover, exploratory experiments on the impact of the used LED were performed (Supplementary Fig. S14). The results displayed that Py-Azine-COF photocatalyst with 2 mol% TEMPO irradiated by LEDs with wavelengths lower than 520 nm accomplished the selective oxidation of methyl phenyl sulfide. Additionally, white LEDs with continuous wavelength enabled the highly selective generation of methyl phenyl sulfoxide with a conversion of 57% and an excellent selectivity. In terms of photocatalytic efficiency, 460 nm blue LEDs were accepted for following experiments. The light-emitting spectrum of the blue LED is also shown (Supplementary Fig. S15).

Subsequently, several essential control tests confirmed that the

presence of light and O_2 is the precondition for the selective conversion of methyl phenyl sulfide (Fig. 5b). Also, 0.1 MPa O_2 was more favorable to generate methyl phenyl sulfoxide than air. In addition, TFPPy hardly drove the transformation of methyl phenyl sulfoxide, obtaining a conversion of 7% in 0.1 MPa O_2 within 1.5 h. Besides, 2 mol% TEMPO as an oxidant was incapable of driving the generation of methyl phenyl sulfoxide alone. However, with the assistance of 2 mol% TEMPO, TFPPy enabled the selective generation of methyl phenyl sulfoxide, in which a conversion of 37% and a selectivity of 97% were obtained. Nevertheless, with the assistance of 2 mol% TEMPO, highly crystalline Py-Azine-COF photocatalyst exhibited more than twice that of TFPPy. Besides, the excellent performance of Py-Azine-COF with TEMPO was also demonstrated by comparing with other representative photocatalysts for the selective oxidation of methyl phenyl sulfide (Supplementary Table S2). Further, the produced ROS in the photocatalytic system of Py-Azine-COF with TEMPO in the selective generation of methyl phenyl sulfoxide was studied (Fig. 5b). The use of CH_3OH as solvent averts the possibility of the generation of hydroxyl radical. Meanwhile, methanol-d₄ (CD_3OD) as an alternative solvent did not present a more desirable result than CH_3OH , thereby excluding the contribution of singlet oxygen (1O_2). However, the separate addition of 1 equiv. KI or $AgNO_3$, or 0.2 equiv. *p*-benzoquinone (*p*-BQ), gave rise to the sharp drop in the conversion of methyl phenyl sulfide. This phenomenon proves that holes, electrons, and O_2^- play crucial roles in the generation of methyl phenyl sulfoxide.

Moreover, the emergence of electrons and O_2^- was confirmed by the electron paramagnetic resonance (EPR) spectra (Supplementary Fig. S16). Photoexcited electrons were gradually formed and accumulated under blue light irradiation. This was indicated by the emergence and ensuing increase of the EPR signal of the electrons. The injection of air resulted in the disappearance of the EPR signal of the electrons, implying that O_2 was activated to ROS, which is probably O_2^- generated by electron transfer. As expected, adopting 5,5-dimethyl-1-pyrroline *N*-oxide (DMPO) as a spin trap reagent, the EPR signal of DMPO- O_2^- appeared and increased with the irradiation time. After turning off the light source, the intensity of the EPR signal of the DMPO- O_2^- decreased slightly. This result indicated that O_2^- is continuously generated and accumulated under light irradiation. Owing to the consumption of O_2^- , the turnoff of the light source caused EPR signal decay. This discovery highlights the crucial contribution of O_2^- as ROS in the selective generation of methyl phenyl sulfoxide. Meanwhile, when 4-oxo-2,2,6,6-tetramethylpiperidine (4-oxo-TEMP) was adopted as a spin probe, the EPR

Table 1

Selective oxidation of organic sulfides with O₂ over Py-Azine-COF photocatalyst with TEMPO^a.

Entry	Substrate	Product	t (h)	Conv. (%)	Sel. (%)
1			1.5	93	98
2 ^b			3.5	95	98
3			1.5	98	98
4			1.0	96	98
5			2.3	91	98
6			1.4	93	98
7			1.9	92	97
8			2.7	93	97
9			2.7	94	96
10			2.7	92	96

Table 1 (continued)

Entry	Substrate	Product	t (h)	Conv. (%)	Sel. (%)
11			2.9	93	97
12			4.3	94	99
13			1.9	96	91
14			2.9	90	95
15			8.0	36	99
16			0.5	96	98
17			0.6	99	97

^a Reaction conditions: Py-Azine-COF (5 mg), CH₃OH (1 mL), TEMPO (6 μmol), sulfide (0.3 mmol), blue LEDs ($\lambda_p = 460$ nm), O₂ (0.1 MPa).

^b Sulfide (0.6 mmol).

signal of 4-oxo-2,2,6,6-tetramethylpiperidine-N-oxyl formed by trapping ¹O₂ with 4-oxo-TEMP enhanced gradually with the extension of irradiation time. Nevertheless, when light was removed, the EPR signal was not weakened. Taking ROS quenchings into consideration, ¹O₂ was unambiguously generated but did not participate in achieving the selective generation of methyl phenyl sulfoxide. Besides, the role of TEMPO was studied in detail. It was found that the EPR signal intensity of TEMPO declined distinctly under blue light irradiation. This situation was aggravated with the extension of irradiation time. However, the turnoff of the light allowed the intensity of the EPR signal to recover, suggesting that TEMPO is crucially involved in the selective oxidation of methyl phenyl sulfide. This also verified that evolution of TEMPO/TEMPO⁺ mediates the hole transfer.

In this case, a mechanism for selective oxidation of methyl phenyl sulfide over Py-Azine-COF photocatalyst with TEMPO is proposed (Scheme 2). Under blue light irradiation, abundant photogenerated holes and electrons are afforded over Py-Azine-COF. As a hole mediator, TEMPO captures the generated hole to be converted into TEMPO⁺. Subsequently, TEMPO⁺ returns to its original state to close its catalytic

cycle by acquiring an electron from methyl phenyl sulfide, giving rise to furnishing S-centered radical cation. Simultaneously, the activation of O₂ occurs over Py-Azine-COF photocatalyst via an electron transfer pathway. The nucleophilic attack of S-centered radical cation by O₂^{•-} enables the further generation of methyl phenyl persulfoxide. At last, CH₃OH drives the generation of the desired methyl phenyl sulfoxide from methyl phenyl persulfoxide.

3.3. Applicability toward the oxidation of organic sulfides

Encouraged by the above results, the applicability of Py-Azine-COF photocatalyst with 2 mol% TEMPO for selective oxidation of sulfides was explored (Table 1). Most of the organic sulfides could be converted to the desirable organic sulfoxides. High conversions and satisfactory selectivities were achieved over Py-Azine-COF photocatalyst with TEMPO. Delightedly, the conversion of 0.6 mmol of methyl phenyl sulfide was completed over Py-Azine-COF photocatalyst with 2 mol% TEMPO in 3.5 h without lowering the excellent selectivity (Table 1, entry 2). Besides, the steric and electronic effects affected the conversions prominently. For the conversions of methyl phenyl sulfides with electron-donating groups ($-CH_3$ and $-OCH_3$) at the *para*-position, a shorter time was required to achieve comparable results smoothly (Table 1, entries 3 and 4). Whereas for the conversions of methyl phenyl sulfides with electron-withdrawing groups ($-F$, $-Cl$, $-Br$, and $-I$) at the *para*-position, a longer time was needed to achieve comparable conversions (Table 1, entries 7–10). The different substitution positions of $-OCH_3$ and $-Cl$, like the *meta*- and *ortho*-positions, also tended to lead to opposite effects (Table 1, entries 5, 6, 11, and 12). With the assistance of 2 mol% TEMPO, Py-Azine-COF photocatalyst was also suitable for the transformations of ethyl phenyl sulfide and 2-(methylthio)naphthalene even with a slight decrease of product selectivities (Table 1, entries 13 and 14). Nonetheless, although diphenylsulfane was well tolerant to the present protocol, only the conversion of 36% was achieved within 8 h, maintaining the high selectivity (Table 1, entry 15). Gratifyingly, some aliphatic sulfides like pentamethylene sulfide and di-*n*-butyl (*n*-Bu) sulfide were compatible with the photocatalytic system, achieving comparable conversions in only 0.5 and 0.6 h, respectively (Table 1, entries 16 and 17). Conclusively, good applicability for Py-Azine-COF photocatalyst with 2 mol% TEMPO was disclosed for the selective oxidation of various sulfides with O₂.

4. Conclusions

In summary, Py-Azine-COF has been constructed by the aldimine condensation between TFPPy and hydrazine hydrate using CF₃COOH as the catalyst. Py-Azine-COF possessed an eclipsed AA stacking, high crystallinity, and a remarkable specific surface area. Intriguingly, selective conversions of organic sulfides were achieved over Py-Azine-COF photocatalyst with TEMPO under blue light irradiation. In essence, TEMPO accelerated the hole transfer over photoexcited Py-Azine-COF and cooperated with O₂^{•-} formed by the electron transfer from O₂, achieving selective oxidation of organic sulfides. With the assistance of 2 mol% TEMPO, the performance of Py-Azine-COF photocatalyst was increased markedly. Gratifyingly, TEMPO, a hole mediator, enabled the expeditious conversions of various organic sulfides into sulfoxides over Py-Azine-COF photocatalyst in CH₃OH. This work highlights that COFs can be customized by modulating the covalent connection of organic building blocks to meet the requirements for selective aerobic oxidations.

CRediT authorship contribution statement

Xiaoyun Dong: Formal analysis, Investigation, Writing – original draft. **Fulin Zhang:** Formal analysis, Investigation. **Yuxin Wang:** Formal analysis, Investigation. **Fengwei Huang:** Formal analysis, Investigation. **Xianjun Lang:** Conceptualization, Funding acquisition,

Supervision, Writing – review & editing.

Declaration of Competing Interest

The authors declare that they have no known competing financial interests or personal relationships that could have appeared to influence the work reported in this paper.

Data availability

Data will be made available on request.

Acknowledgements

This work was supported by the National Natural Science Foundation of China (Grants 22072108 and 22372124). The numerical calculations were done on the supercomputing system in the Supercomputing Center of Wuhan University. We also acknowledge the Core Facility of Wuhan University and the Center for Electron Microscopy at Wuhan University for materials characterizations.

Appendix A. Supporting information

Supplementary data associated with this article can be found in the online version at doi:10.1016/j.apcatb.2023.123660.

References

- [1] A.P. Côté, A.I. Benin, N.W. Ockwig, M. O'Keeffe, A.J. Matzger, O.M. Yaghi, Porous, crystalline, covalent organic frameworks, *Science* 310 (2005) 1166–1170, <https://doi.org/10.1126/science.1120411>.
- [2] A. Krusenbaum, S. Gratz, G.T. Tighe, L. Borchardt, J.G. Kim, The mechanochemical synthesis of polymers, *Chem. Soc. Rev.* 51 (2022) 2873–2905, <https://doi.org/10.1039/dlcs01093>.
- [3] Y. Cao, M.D. Wang, H.J. Wang, C.Y. Han, F.S. Pan, J. Sun, Covalent organic framework for rechargeable batteries: Mechanisms and properties of ionic conduction, *Adv. Energy Mater.* 12 (2022) 2200057, <https://doi.org/10.1002/aenm.202200057>.
- [4] Q. Guan, L.L. Zhou, Y.B. Dong, Metalated covalent organic frameworks: From synthetic strategies to diverse applications, *Chem. Soc. Rev.* 51 (2022) 6307–6416, <https://doi.org/10.1039/dlcs00983d>.
- [5] T. Zhang, G. Zhang, L. Chen, 2D conjugated covalent organic frameworks: Defined synthesis and tailor-made functions, *Acc. Chem. Res.* 55 (2022) 795–808, <https://doi.org/10.1021/acs.accounts.1c00693>.
- [6] Z.J. Chen, K.O. Kirlikovali, K.B. Idrees, M.C. Wasson, O.K. Farha, Porous materials for hydrogen storage, *Chem* 8 (2022) 693–716, <https://doi.org/10.1016/j.chempr.2022.01.012>.
- [7] D. Luo, M. Li, Q.Y. Ma, G.B. Wen, H.Z. Dou, B.H. Ren, Y.Z. Liu, X. Wang, L.L. Shui, Z.W. Chen, Porous organic polymers for Li-chemistry-based batteries: Functionality and characterization studies, *Chem. Soc. Rev.* 51 (2022) 2917–2938, <https://doi.org/10.1039/dlcs01014j>.
- [8] M.S. Lohse, T. Bein, Covalent organic frameworks: Structures, synthesis, and applications, *Adv. Funct. Mater.* 28 (2018) 1705553, <https://doi.org/10.1002/adfm.201705553>.
- [9] M.H. Liu, Y.X. Liu, J.C. Dong, Y.C. Bai, W.Q. Gao, S.C. Shang, X.Y. Wang, J. H. Kuang, C.S. Du, Y. Zou, J.Y. Chen, Y.Q. Liu, Two-dimensional covalent organic framework films prepared on various substrates through vapor induced conversion, *Nat. Commun.* 13 (2022) 1411, <https://doi.org/10.1038/s41467-022-29050-9>.
- [10] G.L. Xing, L. Chen, Linkages take charge, *Nat. Synth.* 1 (2022) 341–343, <https://doi.org/10.1038/s44160-022-00076-7>.
- [11] H.S. Sasmal, A.K. Mahato, P. Majumder, R. Banerjee, Landscaping covalent organic framework nanomorphologies, *J. Am. Chem. Soc.* 144 (2022) 11482–11498, <https://doi.org/10.1021/jacs.2c02301>.
- [12] M.H. Liu, S. Yang, X.B. Yang, C.X. Cui, G.J. Liu, X.W. Li, J. He, G.Z. Chen, Q. Xu, G. F. Zeng, Post-synthetic modification of covalent organic frameworks for CO₂ electroreduction, *Nat. Commun.* 14 (2023) 3800, <https://doi.org/10.1038/s41467-023-39544-9>.
- [13] X.Y. Wang, L.J. Chen, S.Y. Chong, M.A. Little, Y.Z. Wu, W.H. Zhu, R. Clowes, Y. Yan, M.A. Zwijnenburg, R.S. Sprick, A.I. Cooper, Sulfone-containing covalent organic frameworks for photocatalytic hydrogen evolution from water, *Nat. Chem.* 10 (2018) 1180–1189, <https://doi.org/10.1038/s41557-018-0141-5>.
- [14] S.H. Wu, Y. Pan, H. Lin, L.Y. Li, X.Z. Fu, J.L. Long, Crystalline covalent organic frameworks with tailored linkages for photocatalytic H₂ evolution, *ChemSusChem* 14 (2021) 4958–4972, <https://doi.org/10.1002/cssc.202101625>.
- [15] T. Wang, Y.S. Zhang, Z.F. Wang, Y. Chen, P. Cheng, Z.J. Zhang, Olefin-linked covalent organic frameworks: Synthesis and applications, *Dalton Trans.* 52 (2023) 15178–15192, <https://doi.org/10.1039/d3dt01684f>.

[16] H.X. Lin, C.P. Chen, T.H. Zhou, J. Zhang, Two-dimensional covalent-organic frameworks for photocatalysis: The critical roles of building block and linkage, *Sol. RRL* 2 (2021) 2000458, <https://doi.org/10.1002/solr.202000458>.

[17] Y.L. Zhu, P.W. Xu, X.C. Zhang, D.C. Wu, Emerging porous organic polymers for biomedical applications, *Chem. Soc. Rev.* 51 (2022) 1377–1414, <https://doi.org/10.1039/d1cs00871d>.

[18] M. Lu, M. Zhang, J. Liu, Y.F. Chen, J.P. Liao, M.Y. Yang, Y.P. Cai, S.L. Li, Y.Q. Lan, Covalent organic framework based functional materials: Important catalysts for efficient CO₂ utilization, *Angew. Chem. Int. Ed.* 61 (2022) e202200003, <https://doi.org/10.1002/anie.202200003>.

[19] S.S. Huang, K. Chen, T.T. Li, Porphyrin and phthalocyanine based covalent organic frameworks for electrocatalysis, *Coord. Chem. Rev.* 464 (2022) 214563, <https://doi.org/10.1016/j.ccr.2022.214563>.

[20] D.C. Mei, L.J. Liu, B. Yan, Adsorption of uranium (VI) by metal-organic frameworks and covalent-organic frameworks from water, *Coord. Chem. Rev.* 475 (2023) 214917, <https://doi.org/10.1016/j.ccr.2022.214917>.

[21] J. Zhang, L.S. Liu, C.F. Zheng, W. Li, C.R. Wang, T.S. Wang, Embedded nano spin sensor for in situ probing of gas adsorption inside porous organic frameworks, *Nat. Commun.* 14 (2023) 4922, <https://doi.org/10.1038/s41467-023-40683-2>.

[22] J. Fu, J.Y. Liu, G.H. Zhang, Q.H. Zhu, S.L. Wang, S. Qin, L. He, G.H. Tao, Boost of gas adsorption kinetics of covalent organic frameworks via ionic liquid solution process, *Small* 19 (2023) 2302570, <https://doi.org/10.1002/smll.202302570>.

[23] R.H. Shah, S. Ali, F. Raziq, S. Ali, P.M. Ismail, S.Y. Shah, R. Iqbal, X.Q. Wu, W. D. He, X.T. Zu, A. Zada, Adnan, F. Mabood, A. Vinu, S.H. Jhung, J.B. Yi, L. Qiao, Exploration of metal organic frameworks and covalent organic frameworks for energy-related applications, *Coord. Chem. Rev.* 477 (2023) 214968, <https://doi.org/10.1016/j.ccr.2022.214968>.

[24] H.H. Zhang, C. Gu, M.S. Yao, S. Kitagawa, Hybridization of emerging crystalline porous materials: Synthesis dimensionality and electrochemical energy storage application, *Adv. Energy Mater.* 12 (2022) 2100321, <https://doi.org/10.1002/aenm.202100321>.

[25] Z.J. Zheng, H. Ye, Z.P. Guo, Recent progress on pristine metal/covalent-organic frameworks and their composites for lithium-sulfur batteries, *Energy Environ. Sci.* 14 (2021) 1835–1853, <https://doi.org/10.1039/d0ee03181j>.

[26] Z.J. Yong, T.Y. Ma, Solar-to-H₂O₂ catalyzed by covalent organic frameworks, *Angew. Chem. Int. Ed.* 62 (2023) e202308980, <https://doi.org/10.1002/anie.202308980>.

[27] C.C. Qin, X.D. Wu, L. Tang, X.H. Chen, M. Li, Y. Mou, B. Su, S.B. Wang, C.Y. Feng, J.W. Liu, X.Z. Yuan, Y.L. Zhao, H. Wang, Dual donor-acceptor covalent organic frameworks for hydrogen peroxide photosynthesis, *Nat. Commun.* 14 (2023) 5238, <https://doi.org/10.1038/s41467-023-40991-7>.

[28] H.X. Lin, Y. Liu, Z.R. Wang, L.Y. Ling, H. Huang, Q.H. Li, L.X. Cheng, Y.B. Li, J. L. Zhou, K.F. Wu, J. Zhang, T.H. Zhou, Enhanced CO₂ photoreduction through spontaneous charge separation in end-capping assembly of heterostructured covalent-organic frameworks, *Angew. Chem. Int. Ed.* 61 (2022) e202214142, <https://doi.org/10.1002/anie.202214142>.

[29] P.F. Dong, X.Y. Xu, R.A. Luo, S. Yuan, J. Zhou, J.P. Lei, Postsynthetic annulation of three-dimensional covalent organic frameworks for boosting CO₂ photoreduction, *J. Am. Chem. Soc.* 145 (2023) 15473–15481, <https://doi.org/10.1021/jacs.3c03897>.

[30] G.D. Pan, X.S. Hou, Z.Y. Liu, C.K. Yang, J.L. Long, G.C. Huang, J.H. Bi, Y. Yu, L. Y. Li, The hydration-initiated pathway of water oxidation over photoexcited covalent organic frameworks, *ACS Catal.* 12 (2022) 14911–14917, <https://doi.org/10.1021/acscatal.2c03878>.

[31] X.M. Li, Q.B. Dong, Q.Y. Tian, A. Sial, H. Wang, H.L. Wen, B. Pan, K. Zhang, J. N. Qin, C.Y. Wang, Recent advance in metal- and covalent-organic framework-based photocatalysis for hydrogen evolution, *Mater. Today Chem.* 26 (2022) 101037, <https://doi.org/10.1016/j.mtchem.2022.101037>.

[32] Y.X. Wang, F.W. Huang, W.L. Sheng, X. Miao, X. Li, X.K. Gu, X.J. Lang, Blue light photocatalytic oxidation of sulfides to sulfoxides with oxygen over a thiazole-linked 2D covalent organic framework, *Appl. Catal. B* 338 (2023) 123070, <https://doi.org/10.1016/j.apcatb.2023.123070>.

[33] F.L. Zhang, X.Y. Dong, Y.X. Wang, X.J. Lang, Design and synthesis of a triazine-based sp² carbon-conjugated covalent organic framework for blue light photocatalysis, *Small* 19 (2023) 2302456, <https://doi.org/10.1002/smll.202302456>.

[34] Z.P. Li, J.A. Wang, S. Ma, Z.W. Zhang, Y.F. Zhi, F.C. Zhang, H. Xia, G. Henkelman, X.M. Liu, 2D covalent organic frameworks for photosynthesis of α-trifluoromethylated ketones from aromatic alkenes, *Appl. Catal. B* 310 (2022) 121335, <https://doi.org/10.1016/j.apcatb.2022.121335>.

[35] J.L. Li, Z.W. Zhang, J. Jia, X.M. Liu, Covalent organic frameworks for photocatalytic organic transformation, *Chem. Res. Chin. Univ.* 38 (2022) 275–289, <https://doi.org/10.1007/s40242-022-1434-1>.

[36] G.B. Wang, K.H. Xie, H.P. Xu, Y.J. Wang, F. Zhao, Y. Geng, Y.B. Dong, Covalent organic frameworks and their composites as multifunctional photocatalysts for efficient visible-light induced organic transformations, *Coord. Chem. Rev.* 472 (2022) 214774, <https://doi.org/10.1016/j.ccr.2022.214774>.

[37] Z.W. Li, S. Qiu, Y.R. Song, S.Y. Huang, J.F. Gao, L.C. Sun, J.G. Hou, Engineering single-atom active sites anchored covalent organic frameworks for efficient metallaphotoredox C–N cross-coupling reactions, *Sci. Bull.* 67 (2022) 1971–1981, <https://doi.org/10.1016/j.scib.2022.09.010>.

[38] W. Wu, C.H. Dai, M.M. Wu, Y. Chen, C. Zeng, F. Li, Red-light-driven CO₂ photoreduction into CH₄ and CO enabled by narrow-gap conjugated microporous polymers, *Sol. RRL* 7 (2023) 2200907, <https://doi.org/10.1002/solr.202200907>.

[39] C.Z. Han, S.H. Xiang, P.X. Xie, P.H. Dong, C. Shu, C. Zhang, J.X. Jiang, A universal strategy for boosting hydrogen evolution activity of polymer photocatalysts under visible light by inserting a narrow-band-gap spacer between donor and acceptor, *Adv. Funct. Mater.* 32 (2022) 2109423, <https://doi.org/10.1002/adfm.202109423>.

[40] F.P. Kinik, A. Ortega-Guerrero, D. Ongari, C.P. Ireland, B. Smit, Pyrene-based metal organic frameworks: From synthesis to applications, *Chem. Soc. Rev.* 50 (2021) 3143–3177, <https://doi.org/10.1039/d0cs00424c>.

[41] P.Y. Cai, M. Xu, S.S. Meng, Z.F. Lin, T.H. Yan, H.F. Drake, P. Zhang, J.D. Pang, Z. Y. Gu, H.C. Zhou, Precise spatial-designed metal-organic-framework nanosheets for efficient energy transfer and photocatalysis, *Angew. Chem. Int. Ed.* 60 (2021) 27258–27263, <https://doi.org/10.1002/anie.202111594>.

[42] C. Shu, C.Z. Han, X.Y. Yang, C. Zhang, Y. Chen, S.J. Ren, F. Wang, F. Huang, J. X. Jiang, Boosting the photocatalytic hydrogen evolution activity for D-π-A conjugated microporous polymers by statistical copolymerization, *Adv. Mater.* 33 (2021) 2008498, <https://doi.org/10.1002/adma.202008498>.

[43] Y. Kondo, K. Hino, Y. Kuwahara, K. Mori, H. Yamashita, Photosynthesis of hydrogen peroxide from dioxygen and water using aluminium-based metal-organic framework assembled with porphyrin- and pyrene-based linkers, *J. Mater. Chem. A* 11 (2023) 9530–9537, <https://doi.org/10.1039/d3ta01051a>.

[44] A. Jati, S. Dam, S. Kumar, K. Kumar, B. Maji, A π-conjugated covalent organic framework enables interlocked nickel/photoredox catalysis for light-harvesting cross-coupling reactions, *Chem. Sci.* 14 (2023) 8624–8634, <https://doi.org/10.1039/d3sc02440g>.

[45] Y. Kondo, Y. Kuwahara, K. Mori, H. Yamashita, Design of metal-organic framework catalysts for photocatalytic hydrogen peroxide production, *Chem* 8 (2022) 2924–2938, <https://doi.org/10.1016/j.chempr.2022.10.007>.

[46] N.N. Sun, D.D. Qi, Y.C. Jin, H.L. Wang, C.M. Wang, C. Qu, J.M. Liu, Y.H. Jin, W. Zhang, J.Z. Jiang, Porous pyrene organic cage with unusual absorption bathochromic-shift enables visible light photocatalysis, *CCS Chem.* 3 (2021) 2917–2925, <https://doi.org/10.31635/ccschem.021.202101202>.

[47] F.D. Wang, L.J. Yang, X.X. Wang, Y. Rong, L.B. Yang, C.X. Zhang, F.Y. Yan, Q. L. Wang, Pyrazine-functionalized donor–acceptor covalent organic frameworks for enhanced photocatalytic H₂ evolution with high proton transport, *Small* 19 (2023) 202207421, <https://doi.org/10.1002/smll.202207421>.

[48] Y. Mou, X.D. Wu, C.C. Qin, J.Y. Chen, Y.L. Zhao, L.B. Jiang, C. Zhang, X.Z. Yuan, E. H. Ang, H. Wang, Linkage microenvironment of azoles-related covalent organic frameworks precisely regulates photocatalytic generation of hydrogen peroxide, *Angew. Chem. Int. Ed.* (2023) e202309480, <https://doi.org/10.1002/anie.202309480>.

[49] Y.G. Xiang, W.B. Dong, P. Wang, S.Y. Wang, X. Ding, F. Ichihara, Z. Wang, Y. Wada, S.B. Jin, Y.X. Weng, H. Chen, J.H. Ye, Constructing electron delocalization channels in covalent organic frameworks powering CO₂ photoreduction in water, *Appl. Catal. B* 274 (2020) 119096, <https://doi.org/10.1016/j.apcatb.2020.119096>.

[50] B. Zeng, W.L. Sheng, F.W. Huang, K.K. Zhang, K.H. Xiong, X.J. Lang, Cooperative photocatalysis of hafnium-based metal-organic framework and TEMPO for selective oxidation of sulfides, *Chem. Eng. J.* 474 (2023) 145559, <https://doi.org/10.1016/j.cej.2023.145559>.

[51] X.Y. Dong, F.L. Zhang, F.W. Huang, X.J. Lang, Pyrene-based conjugated microporous polymers for red light-powered oxidation of amines to imines, *Appl. Catal. B* 318 (2022) 121875, <https://doi.org/10.1016/j.apcatb.2022.121875>.

[52] G. Cheng, K.W. Wang, S.Y. Wang, L.P. Guo, Z.J. Wang, J.X. Jiang, B.E. Tan, S. B. Jin, Pyrene-based covalent triazine framework towards high-performance sensing and photocatalysis applications, *Sci. China Mater.* 64 (2021) 149–157, <https://doi.org/10.1007/s10843-020-1352-4>.

[53] Z.S. Xiong, B.B. Sun, H.B. Zou, R.W. Wang, Q.R. Fang, Z.T. Zhang, S.L. Qiu, Amorphous-to-crystalline transformation: General synthesis of hollow structured covalent organic frameworks with high crystallinity, *J. Am. Chem. Soc.* 144 (2022) 6583–6593, <https://doi.org/10.1016/j.jacs.2e02089>.

[54] S. Dalapati, S.B. Jin, J. Gao, Y.H. Xu, A. Nagai, D.L. Jiang, An azine-linked covalent organic framework, *J. Am. Chem. Soc.* 135 (2013) 17310–17313, <https://doi.org/10.1021/ja4103293>.

[55] L. Zhang, J.Q. Fan, Q.Q. Zheng, S.J. Xiao, C.R. Zhang, S.M. Yi, X. Liu, W. Jiang, Q. G. Tan, R.P. Liang, J.D. Qiu, A 2D mesoporous hydrazone covalent organic framework for selective detection and ultrafast recovery of Au(III) from electronic waste, *Chem. Eng. J.* 454 (2023) 140212, <https://doi.org/10.1016/j.cej.2022.140212>.

[56] J.E. Nutting, M. Rafiee, S.S. Stahl, Tetramethylpiperidine N-oxyl (TEMPO), phthalimide N-oxyl (PINO), and related N-oxyl species: Electrochemical properties and their use in electrocatalytic reactions, *Chem. Rev.* 118 (2018) 4834–4885, <https://doi.org/10.1021/cr000763>.

[57] Z.S. Lin, R. Kabe, K. Wang, C. Adachi, Influence of energy gap between charge-transfer and locally excited states on organic long persistence luminescence, *Nat. Commun.* 11 (2020) 191, <https://doi.org/10.1038/s41467-019-14035-y>.

[58] H.J. Yang, R. Zhao, Z. Lu, L.Q. Xiao, L.X. Hou, Recognition of "oxygen-/water-fueled" PET-RAFT protocol matched to covalent organic frameworks, *ACS Catal.* (2023) 2948–2956, <https://doi.org/10.1021/acscatal.2c05591>.

[59] Y.Y. Qian, D.D. Li, Y.L. Han, H.L. Jiang, Photocatalytic molecular oxygen activation by regulating excitonic effects in covalent organic frameworks, *J. Am. Chem. Soc.* 142 (2020) 20763–20771, <https://doi.org/10.1021/jacs.0c09727>.

[60] B. Wu, Y. Liu, Y.X. Zhang, L. Fan, Q.Y. Li, Z.Y. Yu, X.S. Zhao, Y.C. Zheng, X. J. Wang, Molecular engineering of covalent triazine frameworks for highly enhanced photocatalytic aerobic oxidation of sulfides, *J. Mater. Chem. A* 10 (2022) 12489–12496, <https://doi.org/10.1039/d2ta01441f>.

[61] X.N. Zou, D.S. Zhang, T.X. Luan, Q. Li, L. Li, P.Z. Li, Y.L. Zhao, Incorporating photochromic triphenylamine into a zirconium-organic framework for highly

effective photocatalytic aerobic oxidation of sulfides, *ACS Appl. Mater. Interfaces* 13 (2021) 20137–20144, <https://doi.org/10.1021/acsami.1c03083>.

[62] Z.P. Xie, W.B. Wang, X.T. Ke, X. Cai, X. Chen, S.B. Wang, W. Lin, X.C. Wang, A heptazine-based polymer photocatalyst with donor-acceptor configuration to promote exciton dissociation and charge separation, *Appl. Catal. B* 325 (2023) 122312, <https://doi.org/10.1016/j.apcatb.2022.122312>.

[63] Q. Li, X.W. Lan, G.Y. An, L. Ricardez-Sandoval, Z.G. Wang, G.Y. Bai, Visible-light-responsive anthraquinone functionalized covalent organic frameworks for metal-free selective oxidation of sulfides: Effects of morphology and structure, *ACS Catal.* 10 (2020) 6664–6675, <https://doi.org/10.1021/acscatal.0c00290>.

[64] F.W. Huang, Y.X. Wang, X.Y. Dong, X.J. Lang, Merging benzothiophene covalent organic framework photocatalysis with TEMPO for selective oxidation of organic sulfides, *Sci. China Chem.* 66 (2023) 3290–3296, <https://doi.org/10.1007/s11426-023-1644-x>.

[65] X.J. Lang, J.C. Zhao, X.D. Chen, Visible-light-induced photoredox catalysis of dye-sensitized titanium dioxide: Selective aerobic oxidation of organic sulfides, *Angew. Chem. Int. Ed.* 55 (2016) 4697–4700, <https://doi.org/10.1002/anie.201600405>.

[66] M. Hayyan, M.A. Hashim, I.M. AlNashef, Superoxide ion: Generation and chemical implications, *Chem. Rev.* 116 (2016) 3029–3085, <https://doi.org/10.1021/acs.chemrev.5b00407>.